DR. SILVIA RAVERA (Orcid ID : 0000-0002-0803-1042)

PROF. GIAMBATTISTA BONANNO (Orcid ID : 0000-0003-3744-5786)

Article type : Original Article

ALTERED GLUCOSE CATABOLISM IN THE PRESYNAPTIC AND PERISYNAPTIC COMPARTMENTS OF SOD1^{G93A} MOUSE SPINAL CORD AND MOTOR CORTEX INDICATES THAT MITOCHONDRIA ARE THE SITE OF BIOENERGETIC IMBALANCE IN ALS.

Silvia Ravera[1, a], Carola Torazza[1], Tiziana Bonifacino[1], Francesca Provenzano[1], Claudia Rebosio[1], Marco Milanese[1], Cesare Usai[2], Isabella Panfoli[3], Giambattista Bonanno[1, 4].

[1] Department of Pharmacy, Unit of Pharmacology and Toxicology and Center of Excellence for Biomedical Research (CEBR), University of Genoa, 16100 Genoa, Italy

[2] Institute of Biophysics, National Research Council (CNR), 16149, Genoa, Italy

[3] Department of Pharmacy, Laboratory of Biochemistry, University of Genoa, 16132 Genoa, Italy

[4] IRCCS San Martino Policlinic Hospital, 16132 Genoa, Italy

[a] Current affiliation: Department of Experimental Medicine, University of Genoa, 16132 Genoa, Italy

***Corresponding Author:**

Prof. Giambattista Bonanno

University of Genoa, Department of Pharmacy, Unit of Pharmacology and Toxicology

Viale Cembrano 4, 16148 Genoa, Italy.

phone: +39 010 335 2658

fax: +39 010 335 2622

e-mail: bonanno@difar.unige.it

Running title: Glucose catabolism at presynaptic and perisynaptic districts in ALS

Keywords: Gliosomes, Glycolysis, Krebs cycle, Motor Cortex, Spinal Cord, Synaptosomes

Abbreviations: ALS, amyotrophic lateral sclerosis; αKG, alpha-ketoglutarate; BSA, bovine serum albumin; CNS, central nervous system; CS, citrate synthase; G3P, glyceraldehyde-3-phosphate; G6PD, glucose-6-phosphatase dehydrogenase; HK, hexokinase; LDH, lactate dehydrogenase; MDH, malate dehydrogenase; MNs, motor neurons; OAA, oxaloacetate; OxPhos, oxidative phosphorylation; PBS, phosphate-buffered saline; PEP, phosphoenolpyruvate; PFK, phosphofructokinase; PK, pyruvate dehydrogenase; RRID, Research Resource Identifier (scicrunch.org); SOD1, Cu/Zn superoxide dismutase type 1.

ABSTRACT

Amyotrophic lateral sclerosis is an adult-onset neurodegenerative disease that develops due to motor neuron death. Several mechanisms occur supporting neurodegeneration, including mitochondrial dysfunction. Recently, we demonstrated that the synaptosomes from the spinal cord of *SOD1*^{G93A} mice, an *in vitro* model of presynapses, displayed impaired mitochondrial metabolism at early pre-symptomatic stages of the disease, while perisynaptic astrocyte particles, or gliosomes, were characterized by mild energy impairment only at symptomatic stages. This work aimed to understand whether mitochondrial impairment is a consequence of upstream metabolic damage. We analysed the critical pathways involved in glucose catabolism at presynaptic and perisynaptic compartments.

Spinal cord and motor cortex synaptosomes from *SOD1*^{G93A} mice displayed high activity of hexokinase and phosphofructokinase, key glycolysis enzymes, and of citrate synthase and malate dehydrogenase, key Krebs cycle enzymes, but did not display high lactate dehydrogenase activity, the key enzyme in lactate fermentation. This enhancement was evident in the spinal cord from the early stages of the disease and in the motor cortex at only symptomatic stages. Conversely, an increase in glycolysis and lactate fermentation activity, but not Krebs cycle activity, was observed in gliosomes from the spinal cord and motor cortex of *SOD1*^{G93A} mice although only at the symptomatic stages of the disease. The cited enzymatic activities were enhanced in spinal cord and motor cortex homogenates, paralleling the time-course of the effect observed in synaptosomes and gliosomes.

The observed metabolic modifications might be considered an attempt to restore altered energetic balance and indicate that mitochondria represent the ultimate site of bioenergetic impairment.

INTRODUCTION

Amyotrophic lateral sclerosis (ALS) is an adult-onset neurodegenerative disease that results in muscle weakness and spasticity due to the selective and progressive degeneration of cortical, brainstem and spinal motor neurons (MNs) (Eisen 2009; Brown and Al-Chalabi 2017). The death of patients with ALS often happens as a result of respiratory failure that usually occurs within 3-5 years after diagnosis (Rowland and Shneider 2001; Turner *et al.* 2013). ALS may develop in two different forms, sporadic (sALS) and familial (fALS); the latter form represents 5-10% of the whole patient population (Swinnen and Robberecht 2014). Even though over 120 potential genes have been identified as possible causes of ALS (Vandoorne *et al.* 2018), approximately 25% of the total fALS cases are associated with mutations in the gene that encodes Cu/Zn superoxide dismutase type 1 (SOD1). More than 100 distinct SOD1 mutations have been identified (Kaur *et al.* 2016), and one of the most abundant SOD1 mutations is the substitution of the glycine at position 93 with alanine (G93A), that was the firstly characterized SOD1 mutation linked to ALS (Gurney *et al.* 1994). For this reason, mice that express the *SOD1*^{G93A} mutation are currently the most common animal model used to study human ALS (Philips and Rothstein 2015).

At present, only two drugs are available: riluzole and edavarone. The first drug increases the survival of patients by a few months, but there is no clear evidence that it ameliorates quality of life (Lu *et al.* 2016), and the second drug is only effective in patients suffering from early-stage ALS (Abe *et al.* 2017); thus, the need for more efficacious therapies is urgent. However, ALS is a very heterogeneous disorder, with many biological alterations that occur, often concomitantly, during disease progression, making it difficult to find a cure. These biological alterations include glutamate-mediated excitotoxicity, oxidative stress, protein aggregation, mitochondrial dysfunction, impaired axonal transport, neuroinflammation,

dysregulated RNA signalling, immunological imbalance, and environmental stress response (Callaghan *et al.* 2011; Ferraiuolo *et al.* 2011; King *et al.* 2016; Peters *et al.* 2015; Tan *et al.* 2014; Lysogorskaia *et al.* 2012; Van Den Bosch *et al.* 2006).

In particular, mitochondrial dysfunction and energy production impairment have been proposed as two of the molecular mechanisms that explain MN degeneration (Vandoorne *et al.* 2018; Carrì *et al.* 2015; Tan *et al.* 2014). In fact, alterations in oxidative phosphorylation (OxPhos) metabolism have been observed both in mouse models and in patients (Mattiazzi *et al.* 2002; Kawamata and Manfredi 2010; Ferri *et al.* 2008; Cozzolino *et al.* 2009), as well as before the clinical onset of ALS pathology (Browne *et al.* 2006). Metabolic alterations have been described both in brain and spinal cord cells (Wiedemann *et al.* 2002; Borthwick *et al.* 1999) as well as in skeletal muscle and liver (Martin 2011), in which the activity of the respiratory electron transport chain and relative ATP synthesis are impaired. Moreover, mitochondrial fusion and fission processes appeared dysfunctional, increasing the damage to energy production (Sasaki and Iwata 1999; Menzies *et al.* 2002a; Jiang *et al.* 2015).

Although MNs are considered the principal target in ALS, astrocytes, microglia, and oligodendrocytes are also involved in the etiopathogenesis of ALS, suggesting that ALS is a non-cell autonomous disease (Ilieva *et al.* 2009; Haidet-Phillips *et al.* 2011). The bioenergetic interactions between astrocytes and the neighbouring MNs are altered in ALS (Allen and Barres 2005; Bilsland *et al.* 2008), and $SOD1^{G93A}$ mouse-derived astrocytes can induce defects in the mitochondria of MNs and reduce neuronal survival (Nagai *et al.* 2007; Bilsland *et al.* 2008; Cassina *et al.* 2008). In addition, *in vitro* studies showed that mitochondrial dysfunction in astrocytes is associated with free radical production and release, which contribute to MN dysfunction in the $SOD1^{G93A}$ mouse model of ALS (Cassina *et al.* 2008; Nagai *et al.* 2007).

Moreover, investigating the glucose catabolism upstream the mitochondrial respiration in muscle of *SOD1*^{G86R} and *SOD1*^{G93A} mice, an impairment of the enzymatic activities involved in glycolysis and the Krebs cycle has been observed (Palamiuc *et al.* 2015; Tefera *et al.* 2016). This dysfunction is associated with a decrease in glucose uptake in numerous brain regions and in the spinal cord of animal models and patients with ALS (Miyazaki *et al.* 2012). Additionally, astrocytes also show decreased lactate release in ALS models compared with control conditions, probably due to altered gene expression of the astrocytic lactate efflux transporter, which contributes to MN degeneration (Ferraiuolo *et al.* 2011). Astrocytes are also considered a key component of the synapse domain due to their essential role in regulating synaptic function, strength and plasticity. Indeed, astrocytes form a well-structured anatomic and functional assembly with the presynaptic and postsynaptic neuronal bodies of the synapse, leading to the widely accepted concept of a tripartite synapse (Perea *et al.* 2009; Papouin *et al.* 2017).

Recently, we demonstrated the presence of alterations in OxPhos metabolism with an *in vitro* model of presynaptic axon terminals and perisynaptic astrocyte processes in *SOD1*^{G93A} mice. In particular, we observed that mitochondrial energy production was differentially impaired in spinal cord axon terminals and perisynaptic astrocyte processes during disease progression, supporting the idea that these two regions may differentially contribute to synaptic damage in ALS (Ravera *et al.* 2018). On the basis of our previous work, in the current study we obtained original data describing the activity of some key enzymes in glycolysis, the Krebs cycle and lactate fermentation (schematically reported in Figure 1) in different synaptic regions, i.e., the presynaptic compartments of neurons and the perisynaptic compartments of astrocytes, to understand whether the observed mitochondrial impairment is a consequence of upstream metabolic damage or is independent of the other pathways involved in energy metabolism.

MATERIALS AND METHODS

Reagents

All reagents are identified by the catalogue number and the year of purchase.

Salts, substrates, and all other chemicals of analytical grade were purchased from Sigma-Aldrich/Merck (St. Louis, MO, USA), including sucrose (Cat# 84097/2017), Tris-HCl (Cat# T3253/2017), Percoll (Cat# P1644/2017), bovine serum albumin (BSA); Cat# 05470/2017), $MgCl_2$ (Cat# M8266/2016), glucose (Cat# G7528/2016), ATP (Cat# A2383/2017), NADP (Cat# N5755/2017), glucose-6-phosphatase dehydrogenase (G6PD); Cat# G5760/2017), KCl (Cat# P9333/2016), fructose 6-phosphate (Cat# F3627/2017), phosphoenolpyruvate (PEP); Cat# P0564/2017), NADH (Cat# N8129/2017), pyruvate kinase (PK); lactate dehydrogenase (LDH) mix (Cat# P0294/2017), pyruvate (Cat# P8574/2017), oxaloacetic acid (Cat# O7753/2017), and acetyl CoA (Cat# A2056/2017).

Ultrapure water (Milli-Q; Millipore, Billerica, MA, USA) was used throughout this study. Safety precautions were taken for chemical hazards in carrying out the experiments.

Animals

B6SJL-TgN SOD1/G93A(+)1Gur mice expressing a high copy number of mutant human SOD1 with a $Gly^{93}Ala$ substitution (*SOD1*^{G93A}; RRID: MGI:4829804) and B6SJL-TgN (SOD1)2Gur mice expressing wild-type human SOD1 (*wtSOD1*; Jackson Cat# 002297/2017) (Gurney *et al.* 1994) were originally obtained from Jackson Laboratories (Bar Harbor, ME) and bred at the animal facility of the Pharmacology and Toxicology Unit, Department of Pharmacy in Genoa. Transgenic animals were crossed with background-matched B6SJL wild-type females (RRID: MGI:5652787), and selective breeding maintained each transgene

in the hemizygous state. All transgenic mice were identified by analysing tissue extracts from tail tips as previously described (Bonifacino *et al.* 2017). Tissue was homogenized in phosphate-buffered saline (PBS), freeze/thawed twice and centrifuged at 23,000 x *g* for 15 min at 4°C, and human SOD1 was evaluated by staining for its enzymatic activity after 10% non-denaturing polyacrylamide gel electrophoresis. Animals were housed (6/7 per cage) at constant temperature (22 ± 1°C) and relative humidity (50%) with a regular 12 h-12 h light cycle (light 7 AM-7 PM) throughout the experiments. Food (4RF21 standard diet obtained from Mucedola, Settimo Milanese, Milan, Italy; Cat# 4RF21/2018) and water were freely available. The number of animals of each sex was balanced in each experimental group to avoid bias due to intrinsic sex-related differences. For experimental use, animals were sacrificed at different stages of disease, according to their age (30, 60, 90, and 120 days old). Experiments were carried out in accordance with the guidelines established by the European Communities Council (EU Directive 114 2010/63/EU for animal experiments published on September 22nd, 2010) and the Italian D.L. n. 26/2014 and were approved by the local Ethical Committee and by the Italian Ministry of Health (Project Authorization No.97/2017-PR). All efforts were made to minimize animal suffering and to use only the number of animals necessary to produce reliable results. All the experiments complied with the ARRIVE guidelines. A total of 22 *wtSOD1* and 20 *SOD1*^{G93A} mice were utilized in this study. No blinding procedures were applied in the experiments.

Purification of synaptosomes and gliosomes

wtSOD1 and *SOD1*^{G93A} mice (30, 60, 90, and 120 days old) were euthanized by cervical dislocation, without prior anaesthesia by personnel well-trained with this technique, and the motor cortex and spinal cord were rapidly removed. Synaptosomes and gliosomes were prepared essentially as previously described (Stigliani *et al.* 2006). The tissue was

homogenized in 0.32 M sucrose, buffered at pH 7.4 with Tris-HCl, using a glass-Teflon tissue grinder (clearance 0.25 mm - Potter-Elvehjem VWR International). The homogenate was centrifuged (5 min, 1,000 x *g*) to remove nuclei and debris. The supernatant was harvested and centrifuged at 12,000 x *g* for 10 min, and the pellet was suspended in Tris-buffered 0.32 M sucrose and gently layered on a discontinuous Percoll® gradient (2, 6, 10 and 20% v/v in Tris-buffered 0.32 M sucrose). After centrifugation at 33,500 x *g* for 5 min, the layer between 2 and 6% (gliosomal fraction) and between 10 and 20% (synaptosomal fraction) Percoll® were collected and washed by centrifugation at 20,000 x g for 15 min with PBS. Gliosomal and synaptosomal pellets were suspended in PBS. All of the above procedures were conducted at 4°C. Protein content was measured according to the Bradford assay (Bradford 1976), using BSA as a standard. Enzymatic assays for each set of data were performed only after all samples were collected, allowing for the reaction mixture preparation of the assays to be optimized and avoiding variability due to the preparation of different reaction mixtures.

Confocal microscopy experiments

Purified synaptosomes or gliosomes (40 µg of total protein) obtained from the motor cortex and spinal cord of 30, 60, 90, and 120-day-old SOD1^{G93A} and age-matched *wtSOD1* mice were stratified onto poly-L-lysine pre-treated coverslips and maintained for 45 min at room temperature to allow the samples to settle and stick to the surface. The samples were fixed with 2% paraformaldehyde (15 min), washed with PBS (3x5 min) and permeabilized (5 min) with 0.05% Triton X-100. After washing (3x5 min) with PBS containing 0.5% BSA, the synaptosomes and gliosomes were triple-labelled by an overnight incubation at 4 °C with primary antibodies diluted in PBS containing 3% BSA. The following primary antibodies were used: mouse anti-microtubule associated protein 2 (MAP2; 1:1000, Sigma-Aldrich,

Cat# M1406/2018; RRID: AB_477171); rabbit anti-glial fibrillary acidic protein (GFAP; 1:1000, Sigma-Aldrich, Cat# G4546/2018: RRID: AB_1840895); and goat anti-LDH (1:1000, Chemicon International, Cat# AB1222/2018, RRID:AB_90491). After washing (3x5 min) with PBS containing 0.5% BSA, the synaptosomes and gliosomes were then incubated for 45 min at room temperature with the appropriate secondary antibodies. The following secondary antibodies were used: goat anti-rabbit Alexa Fluor A555-conjugated (ThermoFisher Scientific, Cat# A-21428/2017, RRID:AB_2535849); donkey anti-mouse Alexa Fluor A488-conjugated (ThermoFisher Scientific, Cat# A-21202/2017, RRID:AB_141607); donkey anti-goat Alexa Fluor A647-conjugated (ThermoFisher Scientific, Cat# A-21447/2018, RRID:AB_2535864). Antibodies were diluted 1:2000 in PBS containing 3% BSA. Fluorescence image (512 x 512 x 8 bit) acquisition was performed by a three-channel Leica TCS SP5 laser-scanning confocal microscope equipped with 458, 476, 488, 514, 543 and 633 nm excitation lines through a plan-apochromatic oil immersion objective 63x/1.4. Light collection was optimized according to the combination of the chosen fluorochromes, and sequential channel acquisition was performed to avoid cross-talk. The Leica "LAS AF" software package was used for image acquisition. The quantitative analyses of co-localization and the relative protein expression level were performed by calculating co-localization coefficients (Manders *et al.* 1992).

Glycolytic enzyme assays

Hexokinase (HK; EC 2.7.1.1) and phosphofructokinase (PFK; EC 2.7.1.11) were assayed as markers of the glycolysis pathway at room temperature using 20 µg of the total protein from synaptosomes, gliosomes, or tissue homogenate in a double beam spectrophotometer (UNICAM UV2, Analytical S.n.c., Italy). Enzymatic activity was expressed as international milliunits/mg (mIU/mg), corresponding to the nanomoles of substrate converted in 1 min. The following reaction mixtures were used (Ravera *et al.* 2013): HK, 100 mM Tris-HCl at

pH 7.4, 5 mM $MgCl_2$, 200 mM glucose, 1 mM ATP, 0.91 mM NADP, and 0.55 IU/ml of glucose 6 phosphate dehydrogenase (NADPH molar extinction coefficient was considered to be 6.22 $\wedge 10^{-3}$ M^{-1} cm^{-1} at 340 nm); and PFK, 100 mM Tris-HCl at pH 7.4, 2 mM $MgCl_2$, 5 mM KCl, 2 mM fructose 6-phosphate, 1 mM ATP, 0.5 mM PEP, 0.2 mM NADH, 2 IU/ml PK and LDH mixture (NADH molar extinction coefficient was considered to be 6.22 $\wedge 10^{-3}$ M^{-1} cm^{-1} at 340 nm). HK and PFK were chosen as markers of the glycolytic pathway because they catalyse two irreversible reactions that are distinct from gluconeogenesis, which represents the counterpart of glycolysis. Moreover, HK and PFK are two regulatory points of glycolysis (Berg *et al.* 2002a).

Lactate fermentation assay

LDH (EC 1.1.1.27) was assayed as a marker of lactate fermentation. The reaction mixture contained 100 mM Tris-HCl at pH 7.4, 5 mM pyruvate and 0.2 mM NADH (NADH molar extinction coefficient was considered to be 6.22 $\wedge 10^{-3}$ M^{-1} cm^{-1} at 340 nm). Enzymatic activity was expressed as mIU/mg, LDH was chosen as a marker of lactate fermentation because it is the unique enzyme responsible for the conversion of pyruvate to lactate, the final step of anaerobic glycolysis (Berg *et al.* 2002b).

Krebs cycle enzyme assay

Citrate synthase (CS; EC 4.1.3.7) and malate dehydrogenase (MDH; EC 1.1.1.37) were assayed as markers of the Krebs cycle in 20 µg of the total protein from synaptosomes and gliosomes using a double beam spectrophotometer (UNICAM UV2, Analytical S.n.c., Italy) at room temperature. Enzymatic activity was expressed as mIU/mg. The following reaction mixtures were used (Ravera *et al.* 2013): CS, 100 mM Tris-HCl at pH 8, 0.17 mM oxaloacetic acid, 0.2 mM acetyl CoA (acetyl CoA molar extinction coefficient was 4.5 $\wedge 10^{-3}$

M^{-1} cm^{-1}, at 232 nm); MDH, 100 mM Tris-HCl at pH 7.5, 0.5 mM oxaloacetic acid, and 0.2 mM NADH (NADH molar extinction coefficient was considered to be 6.22 ^10^{-3} M^{-1} cm^{-1}, at 340 nm). CS was chosen as a marker of the Krebs cycle because it is considered to be the regulator of Krebs cycle rate and is inhibited by high concentrations of ATP, acetyl CoA, and NADH, which indicate a high level of energy supply (Krebs 1970). MDH was chosen as the second marker of Krebs cycle functionality because it interacts with the cytochrome bc1 complex and therefore represents an interaction between citric acid cycle enzymes and electron transfer chain complexes, playing a regulatory role in mitochondrial bioenergetics (Wang *et al.* 2010).

Statistics

Data are expressed as the mean ± s.e.m., and p value < 0.05 was considered significant. The normality of the data was verified by the Kolmogorov-Smirnov test. The presence of outliers was determined by the Grubbs' test and no data were excluded. Sample size calculations were not performed. Multiple comparisons were performed using analysis of variance (two-way ANOVA) followed by Bonferroni post hoc test. Sigma Stat (Sigma Stat Software, Inc., San Jose, CA, USA, USA, version 3.5 (2006), registration number 773050002 RRID:SCR_010285) software was used for statistical analyses.

RESULTS

Purity of the synaptosomes and gliosomes preparations isolated from *wtSOD1* and *SOD1^{G93A}* mouse spinal cord and motor cortex

To verify whether the purity of the neuronal and glial preparations could change in *SOD1^{G93A}* mice at different stages of the disease, we performed laser confocal microscopy experiments. Synaptosomes and gliosomes were prepared from mouse spinal cord and motor cortex tissues of 30-, 60-, 90-, and 120-day-old *SOD1^{G93A}* and *wtSOD1* mice by homogenization and purification on a discontinuous Percoll gradient and were immunolabelled with antibodies against MAP2, a selective neuronal marker, anti-GFAP, a selective astrocyte marker, and anti-LDH. Because LDH is a cytosol-localized enzyme, it can be assumed that LDH-positive particles represent re-sealed synaptosomes or gliosomes rather than membrane debris.

Spinal cord synaptosomes were efficiently stained for LDH and MAP2, and gliosomes were stained for LDH and GFAP. Figure 2, Panel A shows representative images of spinal cord synaptosomes, and Figure 2, Panel B shows representative images of spinal cord gliosomes purified from 90-day-old *SOD1^{G93A}* and *wtSOD1* mice. The merged images revealed that the majority (approximately 80%) of the LDH-positive particles were also MAP2-positive in synaptosomes and GFAP-positive in gliosomes. Figure 2, Panels C and D report the quantification of the LDH particles that were also positive for MAP2 or GFAP in synaptosomes or gliosomes, respectively, at the different stages of the disease. No significant differences in the expression of the MAP2 neuronal component or the GFAP-positive contaminating glia component were detected in the synaptosomal samples of *SOD1^{G93A}* and *wtSOD1* mice at any disease stages. The same was true for GFAP expression and for MAP2-labelled neuronal contamination in gliosomes. Additionally, motor cortex synaptosomes were efficiently stained for LDH and MAP2, and motor cortex gliosomes were stained for LDH

and GFAP (Figure 3, Panels A and B for representative images of synaptosomes and gliosomes, respectively, purified from 90-day-old *wtSOD1* or *SOD1*^{G93A} mice). GFAP contamination in synaptosomes and MAP2 contamination in gliosomes were less than 20%. Figure 3, Panels C and D report the quantification of synaptosome and gliosome purity and show that no significant differences in MAP2 and GFAP expression were detected in the synaptosomes or gliosomes of *SOD1*^{G93A} and *wtSOD1* mice at any disease stage.

Thus, disease progression does not modify the degree of purification of synaptosomes and gliosomes from the spinal cord and motor cortex, allowing for the direct comparison of the bioenergetics data obtained in *wtSOD1* and *SOD1*^{G93A} mice.

Krebs cycle activity in synaptosomes and gliosomes isolated from *wtSOD1* and *SOD1*^{G93A} mouse spinal cord

To investigate whether the dysfunctional mitochondrial metabolism previously observed in synaptosomes isolated from *SOD1*^{G93A} mouse spinal cord (Ravera *et al.* 2018) depends on an upstream alteration of the Krebs cycle, we evaluated the activity of CS and MDH in spinal cord homogenates and derived synaptosomes and gliosomes obtained from *SOD1*^{G93A} and *wtSOD1* mice. Synaptosomes displayed a significantly increased activities of both enzymes at the early stage of the pathology in *SOD1*^{G93A} mice compared with *wtSOD1* mice (CS: $p<0.001$, $F_{(3,1,3,16)}=52.138$ at 30, 60, 90 and 120 days of age; MDH: $p<0.001$, $F_{(3,1,3,16)}=17.588$ at 30, 60, 90 and 120 days of age) (Figure 4, Panels A and D). Conversely, in gliosomes, which did not exhibit altered OxPhos metabolism (Ravera *et al.* 2018), the activities of CS and MDH in samples from *SOD1*^{G93A} mice were similar to those of control samples (Figure 4 Panels B and E). The evaluation of CS and MDH activity in the spinal cord homogenate revealed the same trend observed in the synaptosomes, with an increase already visible at 30

days of age (for CS: $p<0.001$, $F_{(3,1,3,16)}=8.375$ at 30, 60, 90 and 120 days of age; for MDH: $p<0.001$, $F_{(3,1,3,16)}=28.867$ at 30, 60, 90 and 120 days of age) (Figure 4 Panels C and F).

Thus, Krebs cycle activity was strongly and precociously increased in spinal cord tissue and derived nerve terminals but not in perisynaptic astrocyte gliosomes in *SOD1*^{G93A} mice compared with *wtSOD1* mice.

Glycolysis activity in synaptosomes and gliosomes isolated from *wtSOD1* and *SOD1*^{G93A} mouse spinal cord

Considering the enhanced Krebs cycle activity (present results) and the high glucose consumption in ALS (Valbuena *et al.* 2017), we also evaluated glycolytic flux by analysing the activity of HK and PFK in spinal cord homogenates and derived synaptosomes and gliosomes obtained from *SOD1*^{G93A} and *wtSOD1* mice.

Compared to controls, both *SOD1*^{G93A} spinal cord synaptosomes (Figure 5, Panels A and D) and homogenate (Figure 5, Panels C and F) showed a significant increase in HK and PFK activity as early as 30 days of age (HK in synaptosomes: $p<0.001$, $F_{(3,1,3,16)}= 58.040$ at 30, 60, 90 and 120 days; HK in homogenate: $p<0.001$, $F_{(3,1,3,16)}= 380.458$ at 30, 60, 90 and 120 days; PFK in synaptosomes: $p<0.001$, $F_{(3,1,3,16)}= 32.976$ at 30, 60, 90 and 120 days; PFK in homogenate: $p<0.001$, $F_{(3,1,3,16)}= 47.574$ at 30, 60, 90 and 120 days). A significant enhancement in the activity of glycolytic enzymes was also observed in gliosomes from the spinal cord of *SOD1*^{G93A} mice compared with those of *wtSOD1* mice (Figure 5, Panels B and E), but only at 90 and 120 days of age (HK: $p<0.001$, $F_{(3,1,3,16)}= 9.264$ at 90 and 120 days; PFK: $p<0.001$, $F_{(3,1,3,16)}= 40.418$ at 90 and 120 days).

Thus, glycolytic flux was increased in the spinal cord tissue and in the derived synaptosomes and gliosomes of *SOD1*^{G93A} mice compared with those of control mice; however, in gliosomes, the enhancement was evident only at the symptomatic stages of the disease.

Lactate fermentation in synaptosomes and gliosomes isolated from *wtSOD1* and *SOD1^{G93A}* mouse spinal cord

Since pyruvate, derived from glycolysis, can be converted either to acetyl CoA (the initial substrate of the Krebs cycle) or to lactate (the final product of lactate fermentation), we also evaluated the activity of LDH in the spinal cord homogenate and derived synaptosomes and gliosomes obtained from *SOD1^{G93A}* and *wtSOD1* mice. As reported in Figure 6, the LDH activity of *SOD1^{G93A}* synaptosomes was similar to that of *wtSOD1* synaptosomes (Panel A). In contrast, the spinal cord gliosomes and homogenate of *SOD1^{G93A}* mice displayed significantly increased LDH activity compared with those of *wtSOD1* mice (Panels B and C, respectively). In particular, this enhancement was evident in gliosomes at 90 and 120 days of age ($p<0.001$, $F_{(3,1,3,16)}= 131.805$ at 90 and 120 days), while in spinal cord homogenate, this enhancement was observed at 60 days of age ($p<0.001$, $F_{(3,1,3,16)}= 233.472$ at 60, 90 and 120 days).

Thus, the lactate fermentation rates of *SOD1^{G93A}* mice were increased in spinal cord gliosomes, and precociously increased in the homogenate but not increased in synaptosomes compared with those of *wtSOD1* mice.

Krebs cycle activity in synaptosomes and gliosomes isolated from *wtSOD1* and *SOD1^{G93A}* mouse motor cortex

ALS progression also involves upper MN damage in the motor cortex. Therefore, we evaluated the activity of CS and MDH, as markers of Krebs cycle efficiency, in this tissue and in synaptosomes and gliosomes derived from *SOD1^{G93A}* and *wtSOD1* mice. Figure 7 shows that the motor cortex synaptosomes (Panels A and D) and homogenate (Panels C and F) from *SOD1^{G93A}* mice displayed increased CS and MDH activity at 90 and 120 days of age

compared with those from *wtSOD1* mice (CS synaptosomes: $p<0.001$, $F_{(3,1,3,16)}= 17.588$ at 90 and 120 days; CS homogenate: $p<0.001$, $F_{(3,1,3,16)}= 28.867$ at 90 and 120 days; MDH synaptosomes: $p<0.001$, $F_{(3,1,3,16)}= 242.607$ at 90 and 120 days; PFK homogenate: $p<0.001$, $F_{(3,1,3,16)}= 21.536$ at 90 and 120 days). Conversely, the gliosomes from the *SOD1*^{G93A} and *wt*SOD1 mice did not show any differences (Panels B and E).

Thus, as observed in the spinal cord, CS and MDH activities increase in motor cortex synaptosomes and homogenate, starting at the symptomatic phase of the disease. Gliosomes do not show these alterations.

Glycolysis activity in synaptosomes and gliosomes isolated from *wtSOD1* and SOD1^{G93A} motor cortex

Figure 8 shows the activity of HK and PFK in motor cortex synaptosomes and gliosomes and in the homogenate from *SOD1*^{G93A} and *wtSOD1* mice. The synaptosomes (Panels A, D), gliosomes (Panels B, E) and tissue homogenate (Panels C, F) from *SOD1*^{G93A} mice displayed significantly increased HK and PFK activities compared with those from *wtSOD1* mice. Specifically, gliosomes showed a significant increase in glycolytic rate only at the symptomatic stages of the disease, as in spinal cord (HK $p<0.001$, $F_{(3,1,3,16)}= 7.014$ at 90 and 120 days; PFK $p<0.001$, $F_{(3,1,3,16)}= 61.899$ at 90 and 120 days). Additionally, synaptosomes and homogenate showed a significant increase in HK and PFK activities at 90 and 120 days, while in the spinal cord, the increase was significant at 30 days of age (see Figure 5) (HK synaptosomes: $p<0.001$, $F_{(3,1,3,16)}= 47.830$ at 90 and 120 days; HK homogenate: $p<0.001$, $F_{(3,1,3,16)}= 11.673$ at 90 and 120 days; PFK synaptosomes: $p<0.001$, $F_{(3,1,3,16)}= 29.871$ at 90 and 120 days; PFK homogenate: $p<0.001$, $F_{(3,1,3,16)}= 43.262$ at 90 and 120 days).

Thus, the glycolytic rate was also increased in the motor cortex of *SOD1*^{G93A} mice compared with that of *wtSOD1* mice, although only at the symptomatic stages of the disease.

Lactate fermentation in synaptosomes and gliosomes isolated from *wtSOD1* and SOD1^{G93A} motor cortex

Figure 9 reports the activity of LDH, a marker of lactate fermentation, in motor cortex synaptosomes and gliosomes and in homogenate from *SOD1*^{G93A} and *wtSOD1* mice. Synaptosomes from *SOD1*^{G93A} mice were similar to those from *wtSOD1* mice (Panel A). In contrast, the gliosomes and homogenate of *SOD1*^{G93A} mice displayed significantly increased LDH activity at 90 and 120 days of age compared with those of *wtSOD1* mice (Panels B and C) (gliosomes $p<0.001$, $F_{(3,1,3,16)}= 58.716$ at 90 and 120 days of age; homogenate $p<0.001$, $F_{(3,1,3,16)}= 46.575$ at 90 and 120 days of age).

Thus, the lactate fermentation rate appeared to be increased in the motor cortex gliosomes and homogenate, but not the synaptosomes, of *wtSOD1* mice compared with those of *wtSOD1* mice, as observed in the spinal cord.

DISCUSSION

The data reported herein represent the first study addressing glucose catabolism in synaptosomes, presynaptic axon terminals, and gliosomes, perisynaptic astrocyte processes, derived from the spinal cord and motor cortex of *SOD1*^{G93A} mice, a widely studied animal model of ALS. Although impaired energy metabolism has already been described in ALS (Menzies *et al.* 2002b; Tan *et al.* 2014; Sasaki and Iwata 2007), much less is known about the distinctive contribution of neurons and glia at the synaptic level.

We focused our attention on the presynaptic and perisynaptic regions on the basis of our previous studies that supported the idea that ALS can be considered a synaptopathy. In fact, the exocytotic release of glutamate from spinal cord synaptosomes is increased in *SOD1*^{G93A}

mice compared with control mice, starting from the early pre-symptomatic stage of the disease, and this effect is sustained by plastic changes in key protein pathways that regulate neurotransmitter release at the nerve terminal level (Milanese *et al.* 2011; Bonifacino *et al.* 2016). Due to the well-documented non-cell autonomous disease features of ALS, which also involve non-neuronal cell, such as astrocytes (Ilieva *et al.* 2009; Haidet-Phillips *et al.* 2011), contributing to MN degeneration, we thought that the bioenergetic failures that occur during disease progression not only at the nerve terminal level but also at the astrocyte perisynaptic moieties, which surely influence synaptic function, were worthy of analysis (Perea *et al.* 2009; Papouin *et al.* 2017).

Synaptosomes and gliosomes represent a unique tool to investigate the bioenergetic signature of the presynaptic and perisynaptic compartments of the tripartite synapse and to reveal changes during the progression of ALS, since these components can be freshly prepared from mouse spinal cord and motor cortex at different stages of the disease. Synaptosomes represent the site of neurotransmitter release and retain most of the characteristics of the nerve terminals *in vivo*, including the presence of functional mitochondria that meet their bioenergetic needs (Raiteri 1983; Whittaker 1993; Ghijsen *et al.* 2003). Gliosomes are a subcellular preparation that originate from astrocytes (Stigliani *et al.* 2006) and that possess the biochemical and functional characteristics of the cells from which they are derived (Nakamura *et al.* 1993; Stigliani *et al.* 2006; Paluzzi *et al.* 2007). Remarkably, gliosomes express proteins involved in the release machinery and vesicles competent for gliotransmitter exocytosis, as well as transmitter receptors and transporters to interact with the neuronal counterparts. Thus, gliosomes are likely representative of the astrocytic regions that surround the synapses, since they are enriched in proteins distinctive of the perisynaptic astrocytic processes (Carney *et al.* 2014).

Given that ALS in *SOD1*^{G93A} mice is characterized by major synaptic structural changes during disease progression and to exclude that these changes could have influenced the efficiency of the purification of synaptosomes and gliosomes and, in turn, affected the metabolic differences observed, we performed confocal microscopy experiments to characterize the purity of spinal cord and motor cortex synaptosomes and gliosomes from *wtSOD1* and *SOD1*^{G93A} mice at the different stages of the disease. Both neuronal and glial particles showed a good grade of purification, confirming results previously found in the same or different brain regions of rat and mouse (Milanese *et al.* 2010; Raiteri *et al.* 2008; Paluzzi *et al.* 2007; Stigliani *et al.* 2006). Most importantly, these data demonstrate that there were no differences in the purity of samples during disease progression. This observation allows us to conclude that the differences in glucose metabolism described here were indeed due to intrinsic changes in neurons and glial cells.

In a recent work (Ravera *et al.* 2018), we demonstrated that mitochondrial metabolism, in terms of OxPhos activity and coupling, is impaired in synaptosomes derived from the spinal cord of *SOD1*^{G93A} mice, indicating a decreases in their energetic capacity, starting at the early pre-symptomatic stages of the disease (30 days of age). Conversely, gliosomes show only a mild reduction in energy capacity and an increase in lipid peroxidation at the symptomatic stages, but do not show impaired mitochondrial metabolism (Ravera *et al.* 2018). Here, we evaluated the activity of some enzymes involved in glycolysis, Krebs cycle and lactate fermentation in synaptosomes and gliosomes derived from the spinal cord and motor cortex of *SOD1*^{G93A} mice, with the aim to investigate whether the mitochondrial dysfunction of synaptosomes and the involvement of gliosomes in altered energy metabolism may depend on an impairment of the upstream glucose catabolism. We selected these metabolic pathways because the Krebs cycle represents the principal source of the reduced coenzymes necessary for mitochondrial OxPhos activity, while glycolysis is the main glucose catabolic pathway

and produces pyruvate, which represents the crossroads between aerobic and anaerobic metabolism. Moreover, lactate fermentation is necessary for the production of lactate, one of the main fuels of the CNS (Fillenz 2005; Mason 2017). The above analyses were also extended to motor cortex and spinal cord tissue homogenates.

The Krebs cycle activity assay showed that the activities of CS and MDH are increased in the synaptosomes derived from the spinal cord of *SOD1*^{G93A} mice compared with those from *wtSOD1* mice beginning at the early stages of the disease, suggesting an attempt to increase the production of reduced coenzymes to enhance the impaired mitochondrial OxPhos activity. This increase of the aerobic metabolism also appeared to be favoured by the enhancement of the glycolysis pathway, as suggested by the increased HK and PFK activity. Interestingly, synaptosomes from the spinal cord of *SOD1*^{G93A} mice did not display an increase in LDH, indicating that the observed enhancement of glycolysis is completely devoted to aerobic metabolism. Conversely, the activity of the Krebs cycle in gliosomes derived from the spinal cord of *SOD1*^{G93A} was similar to that of control mice, while glycolysis and lactate fermentation were increased in *SOD1*^{G93A} compared with control mice, but exclusively at the symptomatic stages of the disease (90 and 120 days of age). These data suggest that synaptosomes and gliosomes show the same energy metabolism as their cellular counterparts (Bélanger *et al.* 2011), i.e., aerobic metabolism for neuron-derived synaptosomes and anaerobic metabolism for astrocyte-derived gliosomes.

Moreover, the results reported herein are in accordance with our previous observation of a decrease in the ATP/AMP ratio in the same region (Ravera *et al.* 2018). The different alterations of synaptosome and gliosome metabolism suggest that the metabolic changes in ALS could be temporally different in tripartite synapses *in situ*, occurring first in the presynaptic and afterward in the perisynaptic regions. In other words, SOD1^{G93A} mouse gliosomes appear to hyperactivate their fermentative metabolism exclusively at the

symptomatic stage of the disease, likely in response to an energy deficit already present at the nerve terminals in the early stages of the disease. However, the metabolic differences between synaptosomes and gliosomes also suggest the existence of two different pathological mechanisms in presynaptic and perisynaptic regions.

The similarities between the time-course of the effect observed in synaptosomes and gliosomes and the effect observed in tissue homogenates suggest that these components may recapitulate changes taking place in the whole cells from which they are derived. Indeed, the activity of HK and PFK, representing glycolysis, and the activities of CS and MDH, representing the Krebs cycle, were increased at the early stages of the disease in both synaptosomes and tissue homogenates. Also, LDH activity was increased in gliosomes and homogenates; however, in the homogenate, this augmentation was evident already at 60 days, while in gliosomes, it increased only from 90 days. This apparent discrepancy may suggest that the activation of lactate fermentation occurs first in the astrocyte soma and subsequently in their processes. In both cases, the increase in lactate production, driven by augmented LDH activity, could be an attempt to provide additional energy support to neurons.

Similar results were observed in motor cortex synaptosomes and gliosomes and in homogenate. However, in the motor cortex, the increase in metabolic activity was evident only at the symptomatic stages of the disease (90 and 120 days of age), both in synaptosomes and gliosomes and in the tissue homogenate, suggesting that the energetic damage in the motor cortex occurs after the damage to the spinal cord. Remarkably, in our previous work, no impaired energy status was observed in synaptosomes and gliosomes isolated from motor cortex (Ravera *et al.* 2018), further supporting the idea that in this brain region, the metabolic alterations may play a minor role, at least at the synaptic level. Interestingly, we previously observed that glutamate release is not modified in the motor cortex synaptosomes from

SOD1^{G93A} mice (Milanese et al., 2011), possibly indicating similarities between energetic impairment and alterations of glutamate transmission.

Notably, the enhanced aerobic metabolism in synaptosomes induced by the production of reduced coenzymes through the Krebs cycle may pose a risk for a system in which mitochondria are dysfunctional. In fact, the accumulation of reduced coenzymes, due to the impairment of OxPhos machinery, can produce reductive stress, often associated with cell degeneration (Zhang *et al.* 2012). This event can be partially reversed by an increase in lactate fermentation, which converts NADH to NAD^+. On the other hand, the increase of glucose catabolism could represent an attempt to compensate for the OxPhos dysfunction.

The literature regarding glucose catabolism in ALS appears conflicting. For instance, Szelechowski et al have described an increase in the expression of Krebs cycle enzymes in MNs from *SOD1*^{G93A} mice compared with those from control mice, despite a reduction in OxPhos efficiency (Szelechowski *et al.* 2018), while Tefera and Borges observed a decrease in oxoglutarate dehydrogenase activity in brain cortex and spinal cord homogenates isolated from *SOD1*^{G93A} mice (Tefera *et al.* 2019), even though it was not associated with a decrement in the content of the Krebs cycle metabolites.

Moreover, deficient glycolysis or Krebs cycle activity has been deeply investigated mainly in muscle homogenates obtained from different ALS murine models (Tefera *et al.* 2016; Palamiuc *et al.* 2015). Therefore, the different energy status results obtained in ALS could depend both on the different tissues and on the different targets investigated. In particular, the evaluation of metabolic intermediates is very difficult to interpret because the change in the content may depend on both the slowing down of the upstream reactions or the acceleration of the downstream reactions.

In conclusion, our original data show an increment of the glucose catabolic pathways upstream the mitochondrial aerobic respiration in SOD1^{G93A} mice. This increment was present even at pre-symptomatic stages of the disease in spinal cord axon terminals; whereas, it was detectable only starting at symptomatic stages in motor cortex axon terminals and in astrocytic perisynaptic regions. The enhancement of glucose catabolism indicates that the impaired energy production in these districts (Ravera *et al.* 2018) is exclusively a consequence of mitochondrial dysfunction, implying that mitochondria represent the first site of the synaptic and possibly non-synaptic bioenergetic impairment in ALS.

```
--Human subjects --
Involves human subjects:
If yes: Informed consent & ethics approval achieved:
=> if yes, please ensure that the info "Informed consent was achieved for all
subjects, and the experiments were approved by the local ethics committee." is
included in the Methods.
```

```
ARRIVE guidelines have been followed:
Yes
=> if it is a Review or Editorial, skip complete sentence => if No, include a
statement: "ARRIVE guidelines were not followed for the following reason:
"
(edit phrasing to form a complete sentence as necessary).
=> if Yes, insert "All experiments were conducted in compliance with the
ARRIVE guidelines." unless it is a Review or Editorial
```

Acknowledgements

The Authors are indebted to Mr. Giuseppe Marazzotta for his help in maintaining the *SOD1*^{G93A} mouse colonies. The authors gratefully acknowledge the undergraduate students Martina Gullace, Francesca Ferrari for their helpful technical support.

Funding

This work was supported by research grants from the Italian Ministry of University (SIR project n. RBSI14B1Z) to MM and from the Motor Neurone Disease Association (project n. April16/848-791) to GB.

Conflict of interest

The authors declare no competing financial interests.

REFERENCES

Abe K., Aoki M., Tsuji S., Itoyama Y., Sobue G., Togo M., Hamada C., et al. (2017) Safety and efficacy of edaravone in well defined patients with amyotrophic lateral sclerosis: a randomised, double-blind, placebo-controlled trial. *Lancet Neurol.* **16**, 505–512.

Allen N. J., Barres B. A. (2005) Signaling between glia and neurons: focus on synaptic plasticity. *Curr. Opin. Neurobiol.* **15**, 542–8.

Bélanger M., Allaman I., Magistretti P. J. (2011) Brain Energy Metabolism: Focus on Astrocyte-Neuron Metabolic Cooperation. *Cell Metab.* **14**, 724–738.

Berg J., Tymoczko J., Stryer L. (2002a) The Glycolytic Pathway Is Tightly Controlled, in *Biochem. 5th Ed.*, (W. H. Freeman and Company, ed). New York.

Berg J., Tymoczko J., Stryer L. (2002b) Glycolysis Is an Energy-Conversion Pathway in Many Organisms., in *Biochem. 5th Ed.*, (Company W. H. F., ed). New York.

Bilsland L. G., Nirmalananthan N., Yip J., Greensmith L., Duchen M. R. (2008) Expression of mutant SOD1 ^{G93A} in astrocytes induces functional deficits in motoneuron mitochondria. *J. Neurochem.* **107**, 1271–1283.

Bonifacino T., Cattaneo L., Gallia E., Puliti A., Melone M., Provenzano F., Bossi S., et al.

(2017) In-vivo effects of knocking-down metabotropic glutamate receptor 5 in the SOD1 G93A mouse model of amyotrophic lateral sclerosis. *Neuropharmacology* **123**, 433–445.

Bonifacino T., Musazzi L., Milanese M., Seguini M., Marte A., Gallia E., Cattaneo L., Onofri F., Popoli M., Bonanno G. (2016) Altered mechanisms underlying the abnormal glutamate release in amyotrophic lateral sclerosis at a pre-symptomatic stage of the disease. *Neurobiol. Dis.* **95**, 122–133.

Borthwick G. M., Johnson M. A., Ince P. G., Shaw P. J., Turnbull D. M. (1999) Mitochondrial enzyme activity in amyotrophic lateral sclerosis: implications for the role of mitochondria in neuronal cell death. *Ann. Neurol.* **46**, 787–90.

Bosch L. Van Den, Damme P. Van, Bogaert E., Robberecht W. (2006) The role of excitotoxicity in the pathogenesis of amyotrophic lateral sclerosis. *Biochim. Biophys. Acta - Mol. Basis Dis.* **1762**, 1068–1082.

Bradford M. M. (1976) A rapid and sensitive method for the quantitation of microgram quantities of protein utilizing the principle of protein-dye binding. *Anal Biochem* **72**, 248–254.

Brown R. H., Al-Chalabi A. (2017) Amyotrophic Lateral Sclerosis. *N. Engl. J. Med.* **377**, 162–172.

Browne S. E., Yang L., DiMauro J. P., Fuller S. W., Licata S. C., Beal M. F. (2006) Bioenergetic abnormalities in discrete cerebral motor pathways presage spinal cord pathology in the G93A SOD1 mouse model of ALS. *Neurobiol. Dis.* **22**, 599–610.

Callaghan B., Feldman D., Gruis K., Feldman E. (2011) The association of exposure to lead, mercury, and selenium and the development of amyotrophic lateral sclerosis and the

epigenetic implications. *Neurodegener. Dis.* **8**, 1–8.

Carney K. E., Milanese M., Nierop P. Van, Li K. W., Oliet S. H. R., Smit A. B., Bonanno G., Verheijen M. H. G. (2014) Proteomic analysis of gliosomes from mouse brain: Identification and investigation of glial membrane proteins. *J. Proteome Res.* **13**, 5918–5927.

Carrì M. T., Valle C., Bozzo F., Cozzolino M. (2015) Oxidative stress and mitochondrial damage: importance in non-SOD1 ALS. *Front. Cell. Neurosci.* **9**, 41.

Cassina P., Cassina A., Pehar M., Castellanos R., Gandelman M., Leon A. de, Robinson K. M., et al. (2008) Mitochondrial Dysfunction in SOD1G93A-Bearing Astrocytes Promotes Motor Neuron Degeneration: Prevention by Mitochondrial-Targeted Antioxidants. *J. Neurosci.* **28**, 4115–4122.

Cozzolino M., Pesaresi M. G., Amori I., Crosio C., Ferri A., Nencini M., Carrì M. T. (2009) Oligomerization of mutant SOD1 in mitochondria of motoneuronal cells drives mitochondrial damage and cell toxicity. *Antioxid. Redox Signal.* **11**, 1547–58.

Eisen A. (2009) Amyotrophic lateral sclerosis-Evolutionary and other perspectives. *Muscle Nerve* **40**, 297–304.

Ferraiuolo L., Kirby J., Grierson A. J., Sendtner M., Shaw P. J. (2011) Molecular pathways of motor neuron injury in amyotrophic lateral sclerosis. *Nat. Rev. Neurol.* **7**, 616–30.

Ferri A., Nencini M., Cozzolino M., Carrara P., Moreno S., Carrì M. T. (2008) Inflammatory cytokines increase mitochondrial damage in motoneuronal cells expressing mutant SOD1. *Neurobiol. Dis.* **32**, 454–60.

Fillenz M. (2005) The role of lactate in brain metabolism. *Neurochem Int* **47**, 413–417.

Ghijsen W. E. J. M., Leenders A. G. M., Lopes da Silva F. H. (2003) Regulation of vesicle

traffic and neurotransmitter release in isolated nerve terminals. *Neurochem. Res.* **28**, 1443–52.

Gurney M. E., Pu H., Chiu A. Y., Dal Canto M. C., Polchow C. Y., Alexander D. D., Caliendo J., Hentati A., Kwon Y. W., Deng H. X. (1994) Motor neuron degeneration in mice that express a human Cu,Zn superoxide dismutase mutation. *Science* **264**, 1772–5.

Haidet-Phillips A. M., Hester M. E., Miranda C. J., Meyer K., Braun L., Frakes A., Song S., et al. (2011) Astrocytes from familial and sporadic ALS patients are toxic to motor neurons. *Nat. Biotechnol.* **29**, 824–828.

Ilieva H., Polymenidou M., Cleveland D. W. (2009) Non?cell autonomous toxicity in neurodegenerative disorders: ALS and beyond. *J. Cell Biol.* **187**, 761–772.

Jiang Z., Wang W., Perry G., Zhu X., Wang X. (2015) Mitochondrial dynamic abnormalities in amyotrophic lateral sclerosis. *Transl. Neurodegener.* **4**, 14.

Kaur S. J., McKeown S. R., Rashid S. (2016) Mutant SOD1 mediated pathogenesis of Amyotrophic Lateral Sclerosis. *Gene* **577**, 109–18.

Kawamata H., Manfredi G. (2010) Mitochondrial dysfunction and intracellular calcium dysregulation in ALS. *Mech. Ageing Dev.* **131**, 517–526.

King A. E., Woodhouse A., Kirkcaldie M. T. K., Vickers J. C. (2016) Excitotoxicity in ALS: Overstimulation, or overreaction? *Exp. Neurol.* **275**, 162–171.

Krebs H. A. (1970) Rate control of the tricarboxylic acid cycle. *Adv. Enzyme Regul.* **8**, 335–353.

Lu H., Le W. D., Xie Y.-Y., Wang X.-P. (2016) Current Therapy of Drugs in Amyotrophic Lateral Sclerosis. *Curr. Neuropharmacol.* **14**, 314–21.

Lysogorskaia E. V., Abramycheva N. Y., Illarioshkin S. N., Zakharova M. N. (2012) The role of RNA metabolism in the pathogenesis of amyotrophic lateral sclerosis. *Neurochem. J.* **6**, 233–238.

Manders E. M., Stap J., Brakenhoff G. J., Driel R. van, Aten J. A. (1992) Dynamics of three-dimensional replication patterns during the S-phase, analysed by double labelling of DNA and confocal microscopy. *J. Cell Sci.* **103 (Pt 3)**, 857–62.

Martin L. J. (2011) Mitochondrial pathobiology in ALS. *J. Bioenerg. Biomembr.* **43**, 569–79.

Mason S. (2017) Lactate Shuttles in Neuroenergetics—Homeostasis, Allostasis and Beyond. *Front. Neurosci.* **11**, 43.

Mattiazzi M., D'Aurelio M., Gajewski C. D., Martushova K., Kiaei M., Beal M. F., Manfredi G. (2002) Mutated human SOD1 causes dysfunction of oxidative phosphorylation in mitochondria of transgenic mice. *J. Biol. Chem.* **277**, 29626–33.

Menzies F. M., Ince P. G., Shaw P. J. (2002a) Mitochondrial involvement in amyotrophic lateral sclerosis. *Neurochem. Int.* **40**, 543–51.

Menzies F. M., Ince P. G., Shaw P. J. (2002b) Mitochondrial involvement in amyotrophic lateral sclerosis. *Neurochem. Int.* **40**, 543–51.

Milanese M., Zappettini S., Jacchetti E., Bonifacino T., Cervetto C., Usai C., Bonanno G. (2010) *In vitro* activation of GAT1 transporters expressed in spinal cord gliosomes stimulates glutamate release that is abnormally elevated in the SOD1/G93A(+) mouse model of amyotrophic lateral sclerosis. *J. Neurochem.* **113**, 489–501.

Milanese M., Zappettini S., Onofri F., Musazzi L., Tardito D., Bonifacino T., Messa M., et al. (2011) Abnormal exocytotic release of glutamate in a mouse model of amyotrophic lateral sclerosis. *J. Neurochem.* **116**, 1028–1042.

Miyazaki K., Masamoto K., Morimoto N., Kurata T., Mimoto T., Obata T., Kanno I., Abe K. (2012) Early and progressive impairment of spinal blood flow-glucose metabolism coupling in motor neuron degeneration of ALS model mice. *J. Cereb. Blood Flow Metab.* **32**, 456–67.

Nagai M., Re D. B., Nagata T., Chalazonitis A., Jessell T. M., Wichterle H., Przedborski S. (2007) Astrocytes expressing ALS-linked mutated SOD1 release factors selectively toxic to motor neurons. *Nat. Neurosci.* **10**, 615–622.

Nakamura Y., Iga K., Shibata T., Shudo M., Kataoka K. (1993) Glial plasmalemmal vesicles: a subcellular fraction from rat hippocampal homogenate distinct from synaptosomes. *Glia* **9**, 48–56.

Palamiuc L., Schlagowski A., Ngo S. T., Vernay A., Dirrig-Grosch S., Henriques A., Boutillier A.-L., et al. (2015) A metabolic switch toward lipid use in glycolytic muscle is an early pathologic event in a mouse model of amyotrophic lateral sclerosis. *EMBO Mol. Med.* **7**, 526–46.

Paluzzi S., Alloisio S., Zappettini S., Milanese M., Raiteri L., Nobile M., Bonanno G. (2007) Adult astroglia is competent for Na^+/Ca^{2+} exchanger-operated exocytotic glutamate release triggered by mild depolarization. *J. Neurochem.* **103**, 1196–1207.

Papouin T., Dunphy J., Tolman M., Foley J. C., Haydon P. G. (2017) Astrocytic control of synaptic function. *Philos. Trans. R. Soc. B Biol. Sci.* **372**, 20160154.

Perea G., Navarrete M., Araque A. (2009) Tripartite synapses: astrocytes process and control synaptic information. *Trends Neurosci.* **32**, 421–431.

Peters O. M., Ghasemi M., Brown R. H. (2015) Emerging mechanisms of molecular pathology in ALS. *J. Clin. Invest.* **125**, 1767–1779.

Philips T., Rothstein J. D. (2015) Rodent Models of Amyotrophic Lateral Sclerosis. *Curr. Protoc. Pharmacol.* **69**, 5.67.1-21.

Raiteri L., Stigliani S., Usai C., Diaspro A., Paluzzi S., Milanese M., Raiteri M., Bonanno G. (2008) Functional expression of release-regulating glycine transporters GLYT1 on GABAergic neurons and GLYT2 on astrocytes in mouse spinal cord. *Neurochem. Int.* **52**, 103–12.

Raiteri M. (1983) Synaptosomes as a tool in the development of new neuroactive drugs. *Rev. Pure Appl. Pharmacol. Sci.* **4**, 65–109.

Ravera S., Bartolucci M., Calzia D., Aluigi M. G., Ramoino P., Morelli A., Panfoli I. (2013) Tricarboxylic acid cycle-sustained oxidative phosphorylation in isolated myelin vesicles. *Biochimie* **95**, 1991–1998.

Ravera S., Bonifacino T., Bartolucci M., Milanese M., Gallia E., Provenzano F., Cortese K., Panfoli I., Bonanno G. (2018) Characterization of the Mitochondrial Aerobic Metabolism in the Pre- and Perisynaptic Districts of the SOD1^{G93A}Mouse Model of Amyotrophic Lateral Sclerosis. *Mol. Neurobiol.*

Rowland L. P., Shneider N. A. (2001) Amyotrophic Lateral Sclerosis. *N. Engl. J. Med.* **344**, 1688–1700.

Sasaki S., Iwata M. (1999) Ultrastructural change of synapses of Betz cells in patients with amyotrophic lateral sclerosis. *Neurosci. Lett.* **268**, 29–32.

Sasaki S., Iwata M. (2007) Mitochondrial Alterations in the Spinal Cord of Patients With Sporadic Amyotrophic Lateral Sclerosis. *J. Neuropathol. Exp. Neurol.* **66**, 10–16.

Stigliani S., Zappettini S., Raiteri L., Passalacqua M., Melloni E., Venturi C., Tacchetti C., Diaspro A., Usai C., Bonanno G. (2006) Glia re-sealed particles freshly prepared from

adult rat brain are competent for exocytotic release of glutamate. *J. Neurochem.* **96**, 656–68.

Swinnen B., Robberecht W. (2014) The phenotypic variability of amyotrophic lateral sclerosis. *Nat. Publ. Gr.* **doi**.

Szelechowski M., Amoedo N., Obre E., Léger C., Allard L., Bonneu M., Claverol S., et al. (2018) Metabolic Reprogramming in Amyotrophic Lateral Sclerosis. *Sci. Rep.* **8**, 3953.

Tan W., Pasinelli P., Trotti D. (2014) Role of mitochondria in mutant SOD1 linked amyotrophic lateral sclerosis. *Biochim. Biophys. Acta - Mol. Basis Dis.* **1842**, 1295–1301.

Tefera T. W., Bartlett K., Tran S. S., Hodson M. P., Borges K. (2019) Impaired Pentose Phosphate Pathway in the Spinal Cord of the hSOD1G93A Mouse Model of Amyotrophic Lateral Sclerosis. *Mol. Neurobiol.*, 1–12.

Tefera T. W., Wong Y., Barkl-Luke M. E., Ngo S. T., Thomas N. K., McDonald T. S., Borges K. (2016) Triheptanoin Protects Motor Neurons and Delays the Onset of Motor Symptoms in a Mouse Model of Amyotrophic Lateral Sclerosis. *PLoS One* **11**, e0161816.

Turner M. R., Bowser R., Bruijn L., Dupuis L., Ludolph A., McGrath M., Manfredi G., et al. (2013) Mechanisms, models and biomarkers in amyotrophic lateral sclerosis. *Amyotroph. Lateral Scler. Front. Degener.* **14**, 19–32.

Valbuena G. N., Tortarolo M., Bendotti C., Cantoni L., Keun H. C. (2017) Altered Metabolic Profiles Associate with Toxicity in SOD1G93A Astrocyte-Neuron Co-Cultures. *Sci. Rep.* **7**, 50.

Vandoorne T., Bock K. De, Bosch L. Van Den (2018) Energy metabolism in ALS: an

underappreciated opportunity? *Acta Neuropathol.* **135**, 489–509.

Wang Q., Yu L., Yu C.-A. (2010) Cross-talk between mitochondrial malate dehydrogenase and the cytochrome bc1 complex. *J. Biol. Chem.* **285**, 10408–14.

Whittaker V. P. (1993) Thirty years of synaptosome research. *J. Neurocytol.* **22**, 735–42.

Wiedemann F. R., Manfredi G., Mawrin C., Beal M. F., Schon E. A. (2002) Mitochondrial DNA and respiratory chain function in spinal cords of ALS patients. *J. Neurochem.* **80**, 616–25.

Zhang H., Limphong P., Pieper J., Liu Q., Rodesch C. K., Christians E., Benjamin I. J. (2012) Glutathione-dependent reductive stress triggers mitochondrial oxidation and cytotoxicity. *FASEB J.* **26**, 1442–51.

FIGURE LEGENDS

Figure 1. Scheme of glucose catabolism

Scheme of glucose catabolism. The glycolytic pathway is presented in blue, the last step of lactate fermentation is presented in violet, and the Krebs cycle is presented in green. In this schematic, the enzymes evaluated in this article are indicated in boxes. Abbreviations: HK, hexokinase; PFK, phosphofructokinase; LDH, lactate dehydrogenase; CS, citrate synthase; MDH, malate dehydrogenase; G3P, glyceraldehyde 3-phosphate; PEP, phosphoenolpyruvate; αKG, alpha-ketoglutarate; OAA, oxaloacetate.

Figure 2. The purity of synaptosomes and gliosomes obtained from the spinal cord of *wtSOD1* and *SOD1^{G93A}* mice

wtSOD1 and age-matched *SOD1^{G93A}* mice were sacrificed at postnatal days 30, 60, 90 and 120. Purified synaptosomes and gliosomes were immunolabelled and analysed by laser confocal microscopy. Panels A and B show representative images triple-stained by Alexa Fluor 555-conjugated anti-MAP2 (blue; neuron specific marker), Alexa Fluor 488-conjugated anti-GFAP (green; astrocyte specific marker), and Alexa Fluor 647-conjugated anti-lactate dehydrogenase (LDH; red; to label the cytosol of sealed particles) purified from 90-day-old *wtSOD1* and *SOD1^{G93A}* mice. The merged panels show the co-expression of MAP2, GFAP and LDH. Scale bar: 100 μm. Panels C and D show the percent of LDH-positive particles that were also positive for MAP2 or GFAP in synaptosomes and gliosomes at different ages. Data are presented as the mean ± s.e.m. of 3 experiments (3 independent animals) per group, each run in triplicate. No significant differences were found (two-way ANOVA followed by Bonferroni post hoc test).

Figure 3. Purity of synaptosomes and gliosomes obtained from the motor cortex of *wtSOD1* and *SOD1^{G93A}* mice

wtSOD1 and age-matched *SOD1^{G93A}* mice were sacrificed at postnatal days 30, 60, 90 and 120. Purified synaptosomes and gliosomes were immunolabelled and analysed by laser confocal microscopy. Panels A and B show representative images triple-stained by Alexa Fluor 555-conjugated anti-MAP2 (blue; neuron specific marker), Alexa Fluor 488-conjugated anti-GFAP (green; astrocyte specific marker), and Alexa Fluor 647-conjugated anti-lactate dehydrogenase (LDH; red; to label the cytosol of sealed particles) purified from 90-day-old *wtSOD1* and *SOD1^{G93A}* mice. The merged panels show the co-expression of MAP2, GFAP and LDH. Scale bar: 100 μm. Panels C and D show the percent of LDH-positive particles that

were also positive for MAP2 or GFAP in synaptosomes and gliosomes at the studied ages. Data are presented as the mean ± s.e.m. of 3 experiments (3 independent animals) per group, each run-in triplicate. No significant differences were found (two-way ANOVA followed by Bonferroni post hoc test).

Figure 4. Activity of citrate synthase and malate dehydrogenase in the spinal cord synaptosomes, gliosomes, and tissue homogenate from *wtSOD1* and *SOD1^{G93A}* mice

The activity of citrate synthase (CS) and malate dehydrogenase (MDH), components of the Krebs cycle, was measured in the spinal cord synaptosomes, gliosomes, and tissue homogenate of *wtSOD1* and *SOD1^{G93A}* mice at different stages of the disease (30, 60, 90 and 120 days of life). The activity of CS in synaptosomes (Panel A), gliosomes (Panel B) and homogenate (Panel C) and the activity of MDH in synaptosomes (Panel D), gliosomes (Panel E) and homogenate (Panel F) are reported. For each enzyme, the data are expressed as international milliunits (mUI), corresponding to the nanomoles of substrate catalysed in 1 min per mg of protein, and are presented as box-plots showing the median, quartiles (boxes) and range (whiskers) of 4 experiments (4 independent animals), each of which were performed in triplicate. * $p<0.01$ vs age-matched *wtSOD1* mice (two-way ANOVA followed by Bonferroni post hoc test).

Figure 5. Activity of hexokinase and phosphofructokinase in the spinal cord synaptosomes gliosomes and tissue homogenate of *wtSOD1* and *SOD1^{G93A}* mice

The activity of hexokinase (HK) and phosphofructokinase (PFK), components of the glycolysis pathway, was measured in the spinal cord synaptosomes, gliosomes, and tissue homogenate of *wtSOD1* and *SOD1^{G93A}* mice at different stages of the disease (30, 60, 90 and 120 days of life). The activity of HK in synaptosomes (Panel A), gliosomes (Panel B) and

homogenate (Panel C) and the activity of PFK in synaptosomes (Panel D), gliosomes (Panel E) and homogenate (Panel F) are reported. For each enzyme, data are expressed as international milliunits (mUI), corresponding to the nanomoles of substrate catalysed in 1 min per mg of protein, and are presented as box-plots showing the median, quartiles (boxes) and range (whiskers) of 4 experiments (4 independent animals), each of which were performed in triplicate* $p<0.01$ vs age-matched *wtSOD1* mice (two-way ANOVA followed by Bonferroni post hoc test).

Figure 6. Activity of lactate dehydrogenase in the spinal cord synaptosomes, gliosomes and tissue homogenate of *wtSOD1* and *SOD1^{G93A}* mice

The activity of lactate dehydrogenase (LDH), a marker of lactate fermentation, was measured in the spinal cord synaptosomes (Panel A), gliosomes (Panel B) and tissue homogenate (Panel C) of *wtSOD1* and *SOD1^{G93A}* mice at different stages of the disease (30, 60, 90 and 120 days of life). Data are expressed as international milliunits (mUI), corresponding to the nanomoles of substrate catalysed in 1 min per mg of protein, and are presented as box-plots showing the median, quartiles (boxes) and range (whiskers) 4 experiments (4 independent animals), each of which were performed in triplicate. * $p<0.01$ vs age-matched *wtSOD1* mice (two-way ANOVA followed by Bonferroni post hoc test).

Figure 7. Activity of citrate synthase and malate dehydrogenase in the motor cortex synaptosomes, gliosomes, and tissue homogenate of *wtSOD1* and *SOD1^{G93A}* mice

The activity of citrate synthase (CS) and malate dehydrogenase (MDH), components of the Krebs cycle, was measured in the motor cortex synaptosomes, gliosomes, and tissue homogenate of *wtSOD1* and *SOD1^{G93A}* mice at different stages of the disease (30, 60, 90 and 120 days of life). The activity of CS in motor cortex synaptosomes (Panel A), gliosomes

(Panel B) and homogenate (Panel C) and the activity of MDH in motor cortex synaptosomes (Panel D), gliosomes (Panel E) and homogenate (Panels F) are reported. For each enzyme, data are expressed as international milliunits (mUI), corresponding to the nanomoles of substrate catalysed in 1 min per mg of protein, and are presented as box-plots showing the median, quartiles (boxes) and range (whiskers) of 4 experiments (4 independent animals), each of which were performed in triplicate. * $p<0.01$ vs age-matched *wtSOD1* mice (two-way ANOVA followed by Bonferroni post hoc test).

Figure 8. Activity of hexokinase and phosphofructokinase in the motor cortex synaptosomes, gliosomes, and tissue homogenate of *wtSOD1* and *SOD1^{G93A}* mice

The activity of hexokinase (HK) and phosphofructokinase (PFK), components of the glycolysis pathway, was measured in the motor cortex synaptosomes, gliosomes and tissue homogenate of *wtSOD1* and *SOD1^{G93A}* mice at different stages of the disease (30, 60, 90 and 120 days of life). The activity of HK in synaptosomes (Panel A), gliosomes (Panel B), and homogenate (Panel C) and the activity of PFK in synaptosomes (Panel D), gliosomes (Panel E) and homogenate (Panel F) are reported. For each enzyme, data are expressed as international milliunits (mUI), corresponding to the nanomoles of substrate catalysed in 1 min per mg of protein, and are presented as box-plots showing the median, quartiles (boxes) and range (whiskers) of 4 experiments (4 independent animals), each of which were performed in triplicate. * $p<0.01$ vs age-matched *wtSOD1* mice (two-way ANOVA followed by Bonferroni post hoc test).

Figure 9. Activity of lactate dehydrogenase in the motor cortex synaptosomes, gliosomes, and tissue homogenate of *wtSOD1* and *SOD1*^{G93A} mice

The activity of lactate dehydrogenase (LDH), a marker of lactate fermentation, was measured in motor cortex synaptosomes (Panel A), gliosomes (Panel B) and tissue homogenate (Panel C) of *wtSOD1* and *SOD1*^{G93A} mice at different stages of the disease (30, 60, 90 and 120 days of life). Data are expressed as international milliunits (mUI), corresponding to the nanomoles of substrate catalysed in 1 min per mg of protein, and are presented as box-plots showing the median, quartiles (boxes) and range (whiskers) of 4 experiments (4 independent animals), each of which was performed in triplicate. * $p<0.01$ vs age-matched *wtSOD1* mice (two-way ANOVA followed by Bonferroni post hoc test).

Figure 1

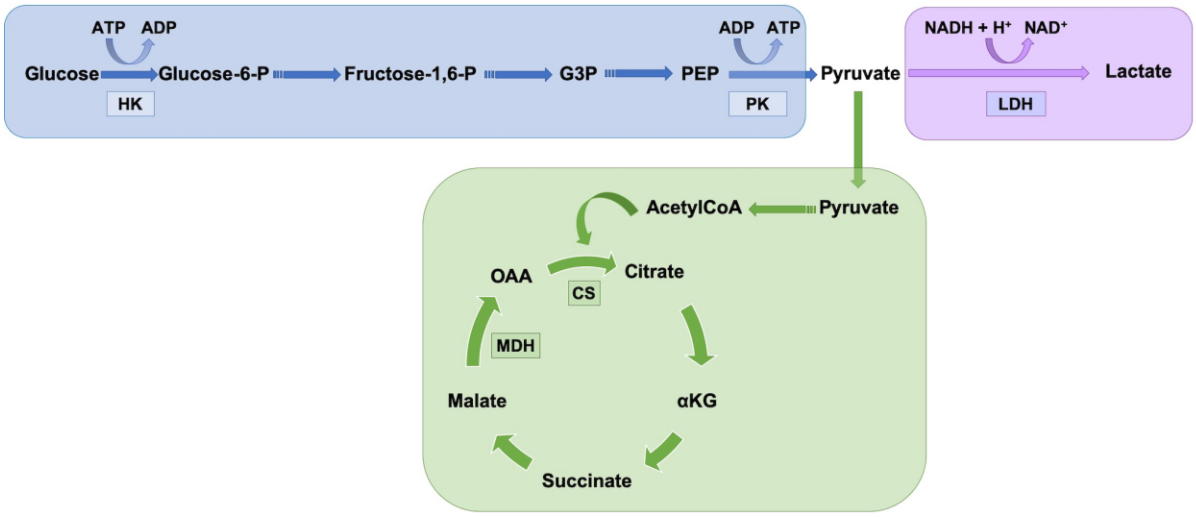

Figure 2

SPINAL CORD

A

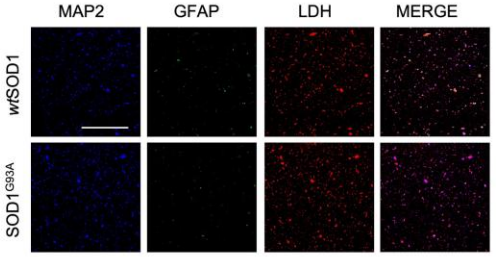

B

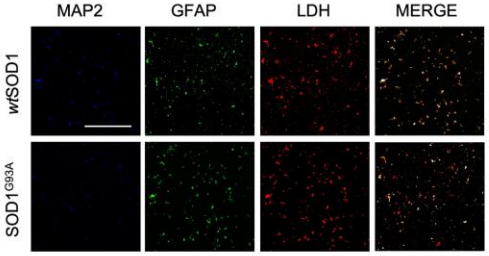

C

	wt SOD1		*SOD1 G93A*	
Days	LDH/MAP2	LDH/GFAP	LDH/MAP2	LDH/GFAP
30	78.3 ± 5.36	29.3 ± 3.33	74.8 ± 3.76	23.2 ± 2.89
60	75.8 ± 3.18	21.7 ± 2.33	72.5 ± 4.06	25.3 ± 1.45
90	78.9 ± 5.55	22.1 ± 1.45	80.0 ± 4.93	22.4 ± 2.33
120	73.6 ± 4.33	22.1 ± 2.52	73.9 ± 4.41	22.0 ± 1.21

D

	wt SOD1		*SOD1 G93A*	
Days	LDH/MAP2	LDH/GFAP	LDH/MAP2	LDH/GFAP
30	27.0 ± 2.00	79.6 ± 3.76	19.5 ± 2.03	79.3 ± 3.53
60	21.6 ± 2.60	83.4 ± 3.53	18.1 ± 4.36	79.8 ± 3.53
90	23.1 ± 4.36	82.8 ± 2.85	21.4 ± 1.45	73.7 ± 3.93
120	21.2 ± 1.53	78.7 ± 3.48	18.7 ± 1.20	77.5 ± 4.41

Figure 3

MOTOR CORTEX

A

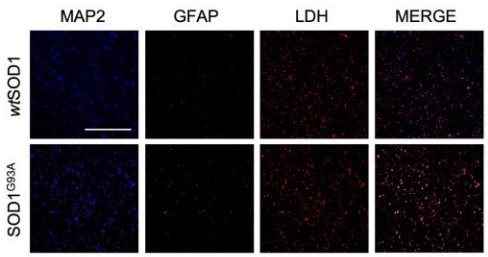

B

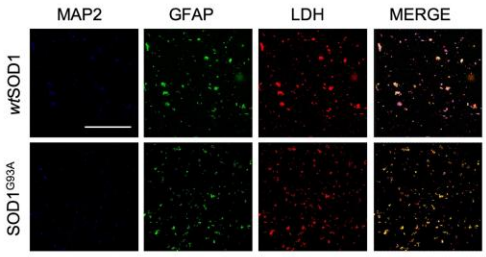

C

	wt SOD1		*SOD1 G93A*	
Days	LDH/MAP2	LDH/GFAP	LDH/MAP2	LDH/GFAP
30	79.3 ± 4.16	19.2 ± 0.88	76.6 ± 4.26	22.3 ± 2.03
60	81.7 ± 5.21	19.0 ± 1.15	74.0 ± 4.93	20. 2 ± 1.76
90	74.9 ± 3.76	18.7 ± 4.67	78.9 ± 3.06	21.0 ± 1.73
120	72.8 ± 4.63	24.7 ± 1.45	71.9 ± 2.91	22.1 ± 1.45

D

	wt SOD1		*SOD1 G93A*	
Days	LDH/MAP2	LDH/GFAP	LDH/MAP2	LDH/GFAP
30	24.2 ± 1.45	84.7 ± 4.33	20.3 ± 2.19	78.4 ± 3.46
60	18.9 ± 4.08	88.6 ± 4.33	19.4 ± 2.08	85.8 ± 5.21
90	26.6 ± 2.96	75.5 ± 3.84	25.2 ± 3.18	81.5 ± 3.38
120	22.8 ± 1.15	80.8 ± 3.48	26.6 ± 1.20	85.1 ± 5.21

Figure 4

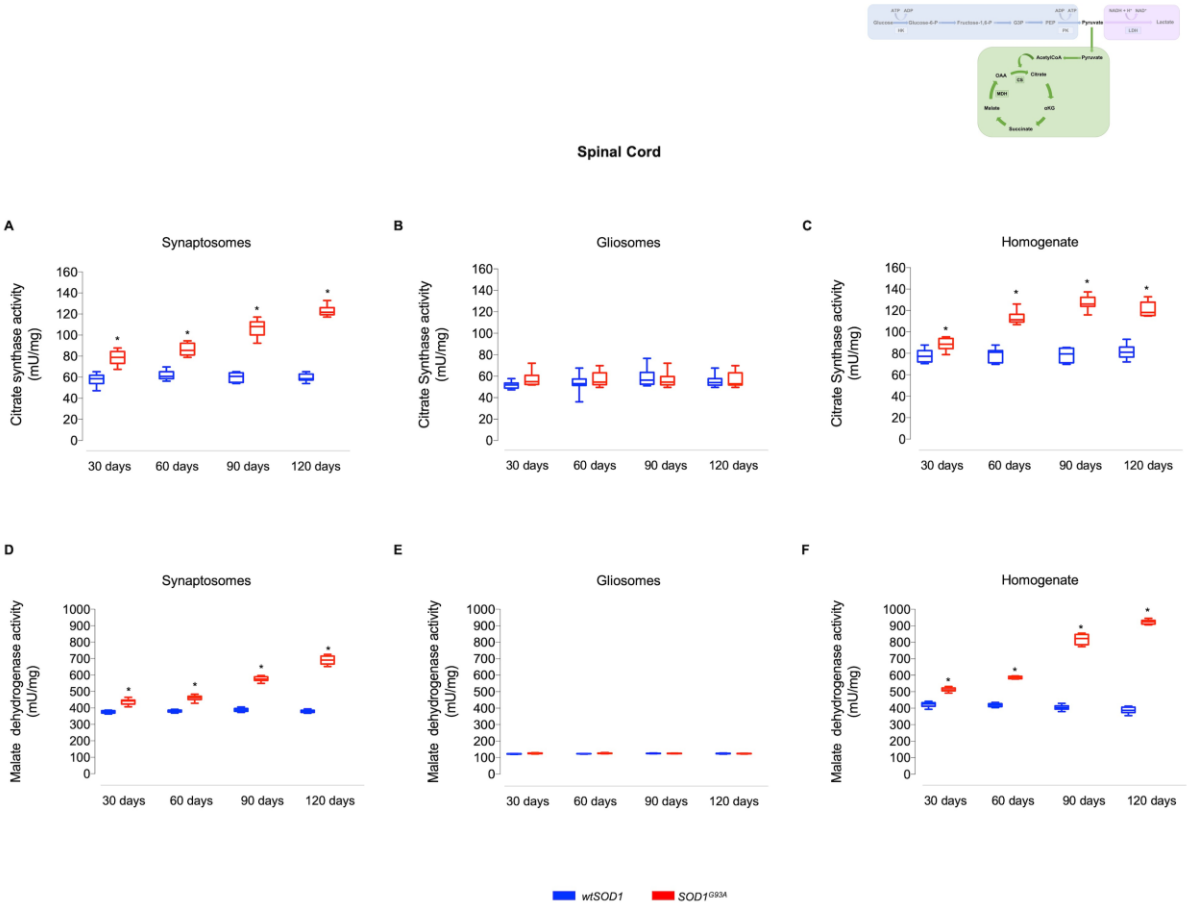

Figure 5

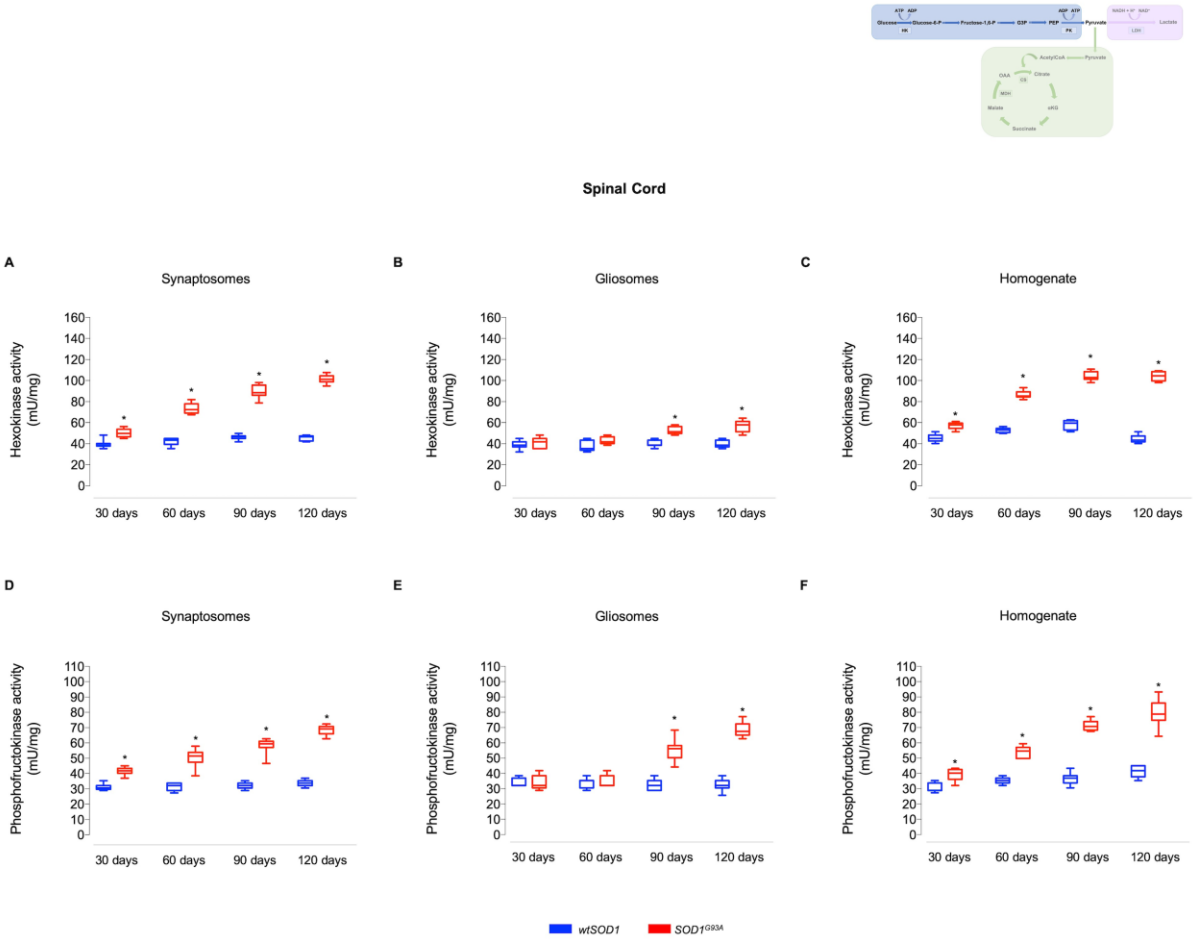

Figure 6

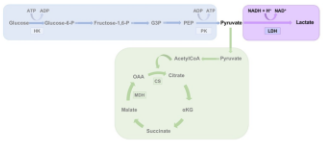

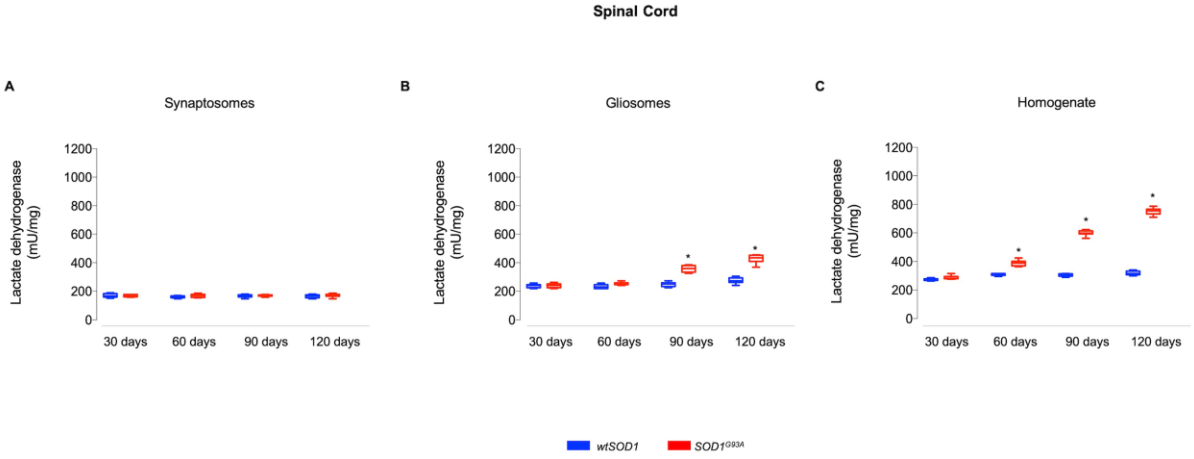

Figure 7

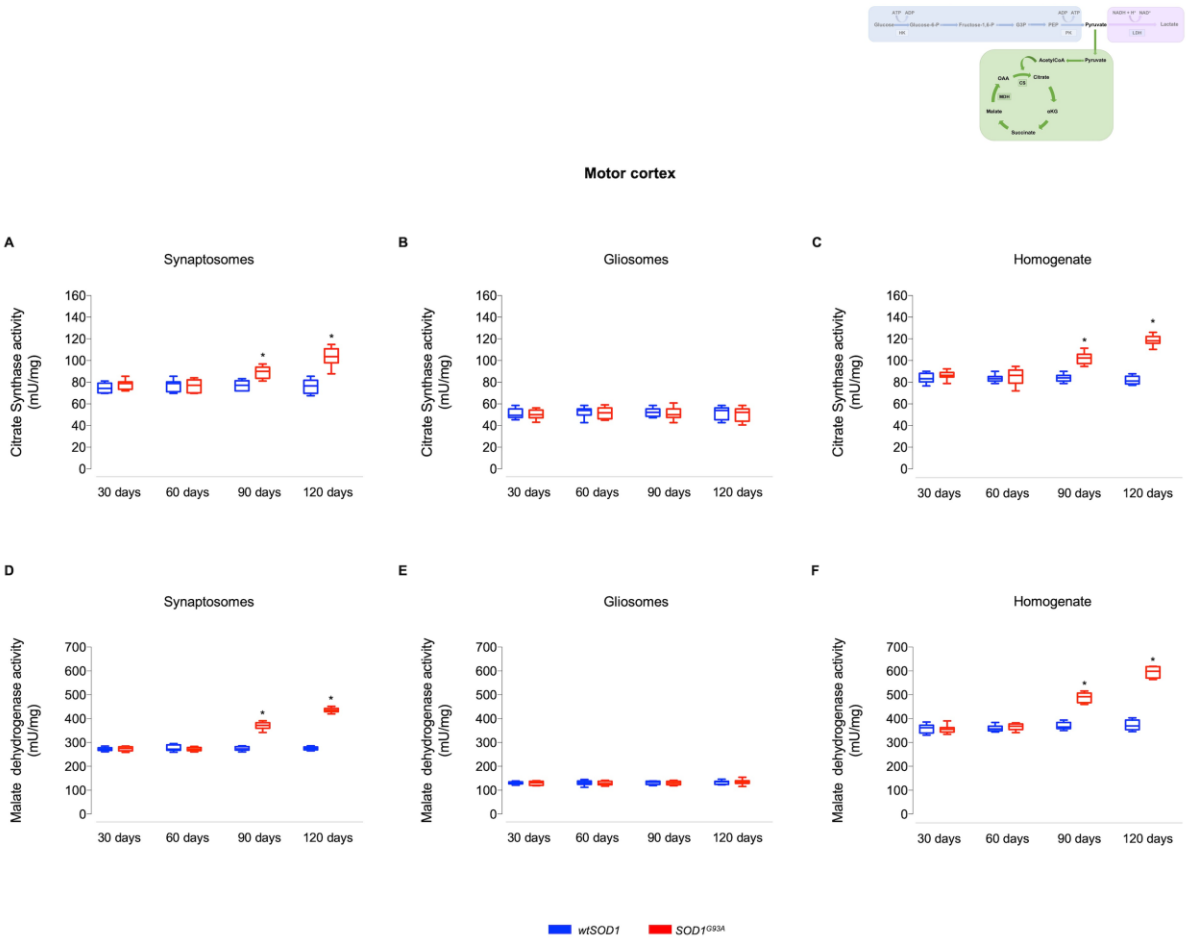

Figure 8

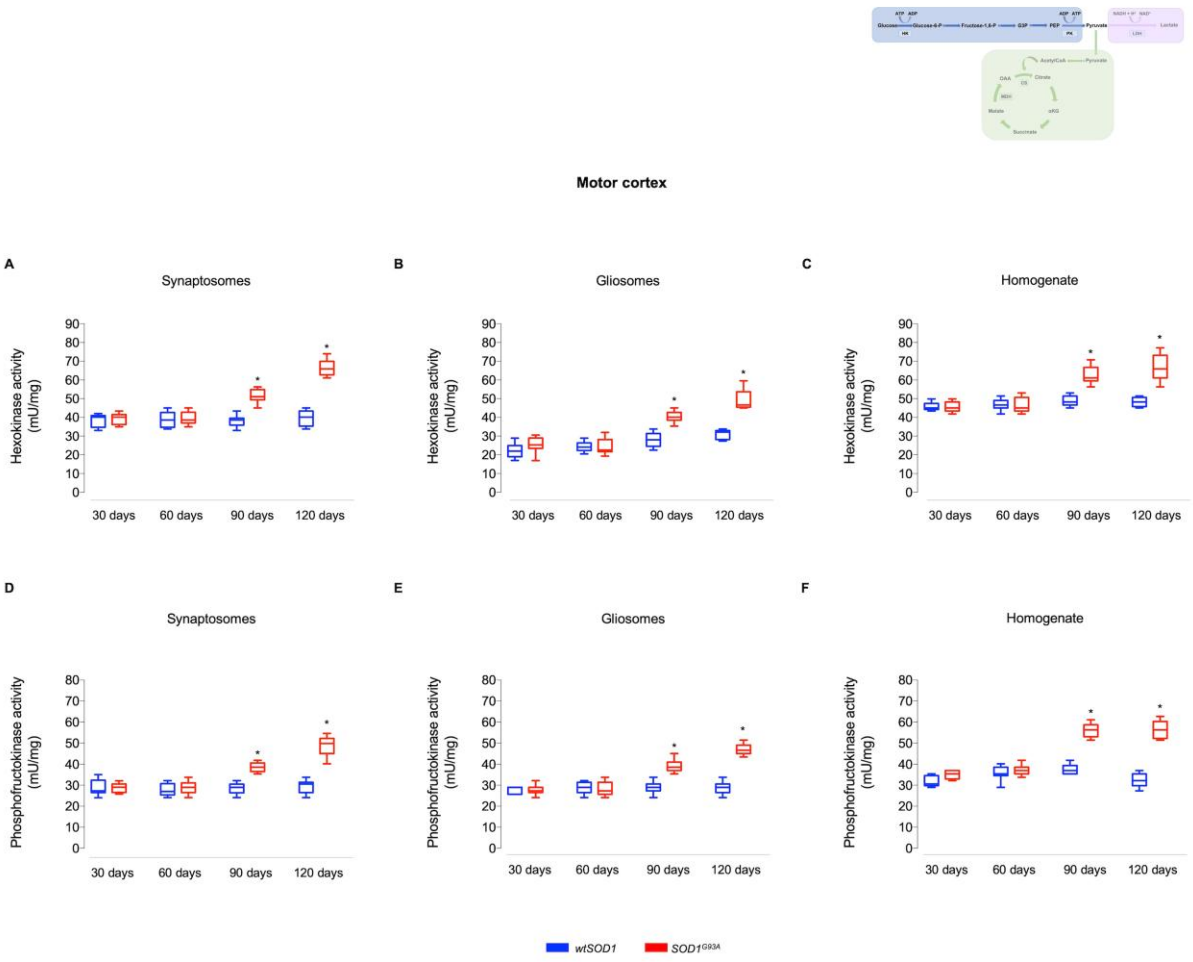

Figure 9